Available online at www.sciencedirect.com

ScienceDirect

Procedia CIRP 101 (2021) 114–117

www.elsevier.com/locate/procedia

9th CIRP Conference on High Performance Cutting (HPC 2020)

Comparative analysis of cutting forces and stability of standard and non-standard profiled serrated end mills

Pritam Bari[a], Mohit Law[a,*], Pankaj Wahi[b]

[a]*Machine Tool Dynamics Laboratory, Department of Mechanical Engineering, Indian Institute of Technology Kanpur, Kanpur 208016, India.*
[b]*Department of Mechanical Engineering, Indian Institute of Technology Kanpur, Kanpur 208016, India.*

* Corresponding author. Tel.: +91-512-679-6897; fax: +91-512-679-7408. *E-mail address:* mlaw@iitk.ac.in

Abstract

The ability of serrated end mills to reduce cutting forces and improve chatter-free machinability is governed by their serration profiles. This paper presents a comparative analysis of the cutting behavior of two differently profiled serrated end mills, of which one has a standard trapezoidal profile, and another has a non-standard inclined-circular profile. Established force and stability models are used to predict the cutting behavior that is experimentally validated. For cutting aluminium, cutting forces for the non-standard inclined-circular cutter are lower than the standard trapezoidal cutter. However, from the chatter-free stability point of view, both cutters perform similarly.

Keywords: Stability; Force; Serrated end milling

1. Introduction

Serrated end mills are widely used for rough machining in the aerospace, automobile, and die-mould industries. Due to complex geometries of the serrated cutters, its local radius varies. This produces a non-uniform chip thickness and an apparent depth of cut, which is different than regular end mills. These variations and differences tend to reduce process forces and improve chatter-free machining stability limits. Improvements in the cutting performance of serrated cutters is mainly influenced by the geometry of the serration profiles.

Superior performance of serrated cutters has spurred great interest in understanding the role of the serration profile on the cutting mechanics and stability of serrated cutters. Based on the early seminal work by Stone [1] and Tlusty et al. [2], several significant contributions to modelling the geometry, process mechanics, and the machining stability of serrated cutters have been made [3-8]. Almost all previously reported work has addressed cutting with standard profiled serrated cutters, wherein the profile is either sinusoidal [1-6], circular, trapezoidal [1, 3-4] and/or of the interrupted circular and trapezoidal kinds [8]. However, as was shown recently [8-9], serration geometrics can also be of the non-standard kinds that can be classified as semi-circular, circular-elliptical, semi-elliptical, inclined semi-circular, and the inclined-circular types. How/if cutting forces and stability of these non-standard cutters is different from standard profiled cutters is yet unknown, and forms the main focus of this paper.

For cutting aluminium, we compare the cutting performance of one standard trapezoidal profiled serrated cutter with another non-standard inclined-circular profiled serrated cutter. To make comparisons meaningful, we present models that are experimentally validated. Section 2 summarizes the static force model, and Section 3 discusses the model for chatter stability for these cutters. Section 4 describes the measured geometry of both cutters, followed by experimental validations in Section 5. Section 6 compares the performance of both cutters, followed by the main conclusions of the paper.

10.1016/j.procir.2021.02.014

2. Static cutting force model for serrated cutters

The static cutting force model used in this study is based on [4-6]. The tool is considered to be rigid herein, and the influence of flexibility is treated separately in the next section. The local radius of the serrated cutter for the i^{th} flute at height z is defined by $R_i(z) = D/2 - \Delta R_i(z)$, wherein D is shank diameter of the cutter and $\Delta R_i(z)$ is the variation in the local radius. The parametric expression of $\Delta R_i(z)$ is well defined in [9] for different kinds of serration profiles. The variation in local radius leads to non-uniform static chip thickness $h_i^{st}(z,t)$ for the i^{th} flute at height z and time t, as is detailed in [4-6].

Due to their complex geometries, serrated cutters are discretized into axial slices, which are in turn further discretized into angular elements. In each element, we attach a radial-tangential-and-axial (*rta*) frame which changes direction from element to element. Using elemental static chip thickness formulations, and by ignoring the influence of runout, static cutting forces are evaluated in the *rta* frame and transformed later into a fixed *xyz* frame as follows:

$$d\boldsymbol{F}^{st}{}_{xyz,i}(z,t) = \boldsymbol{T}_{xr,i}(z,t)[\boldsymbol{K}^c h_i^{st}(z,t) + \boldsymbol{K}^e]\frac{dz}{\sin\kappa_i(z)} g_i(z,t), \quad (1)$$

wherein $g_i(z,t)$ is the screening function, and $\kappa_i(z)$ is the axial immersion angle for the i^{th} flute at height z – shown in Fig. 1(b), $\boldsymbol{K}^c$ and $\boldsymbol{K}^e$ are the main and edge cutting force coefficients vectors, and $\boldsymbol{T}_{xr,i}(z,t)$ is a transformation matrix.

The total lumped static cutting force vector in different directions is calculated from elemental differential forces as:

$$\boldsymbol{F}_{xyz}^{st}(t) = \begin{bmatrix} F_x^{st} & F_y^{st} & F_z^{st} \end{bmatrix}^T \equiv \sum_{i=1}^{N} \int_0^{a_p} d\boldsymbol{F}^{st}{}_{xyz,i}(z,t), \quad (2)$$

wherein a_p is the axial depth of cut, and N represents the number of teeth. For force model details, please see [4-6].

3. Chatter stability model for serrated cutters

In the case of tool being flexible, the dynamic chip thickness governs the chatter stability of the system as described subsequently. The regenerative chatter stability model presented herein is based on the work reported in [6].

3.1. Dynamic chip thickness

Assuming the tool is flexible in three orthogonal directions as shown in Fig. 1, the cutting forces can excite the structure in the feed (x), normal (y), and axial (z) directions thereby resulting in a dynamic displacement in those directions. Using a coordinate transformation from fixed *xyz* to rotating *rta* frame, we calculate local dynamic chip thickness as follows:

$$h_i^{dc}(z,t) = \begin{bmatrix} \sin\varphi_i(z,t)\sin\kappa_i(z) \\ \cos\varphi_i(z,t)\sin\kappa_i(z) \\ \cos\kappa_i(z) \end{bmatrix}^T \begin{bmatrix} \Delta x \\ \Delta y \\ \Delta z \end{bmatrix} \times g_i(z,t) \quad (3)$$

wherein $\Delta x \coloneqq x(t) - x(t - \tau_i(z,t))$, $\Delta y \coloneqq y(t) - y(t - \tau_i(z,t))$, and $\Delta z \coloneqq z(t) - z(t - \tau_i(z,t))$ represents the dynamic displacements in $x, y,$ and z directions, and $\tau_i(z,t)$ is the time delay between current and past vibration marks left on the cutting surfaces. $\varphi_i(z,t)$ in Eq. (3) is the angular immersion angle for the i^{th} flute at height z. For additional details, please see [4-6].

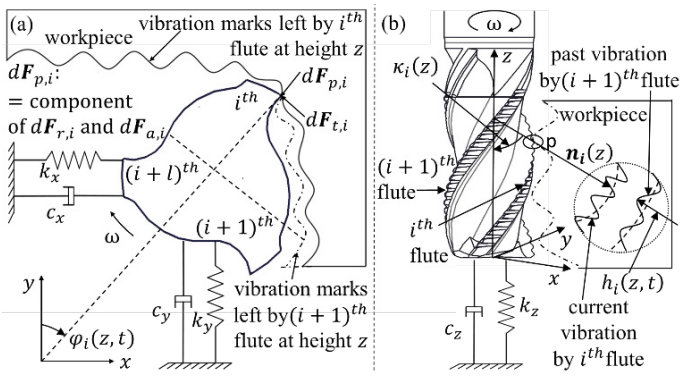

Fig. 1. Schematic of a flexible serrated end mill showing details of the dynamic chip thickness. (a) top view, (b) end view.

Because of the variation in the local radius of these cutters, there can be the missed-cut effect, which disturbs regenerative vibrations and leads to the multiple delay term $\tau_i(z,t)$ [4-6]. Using the dynamic chip thickness defined in Eq. (3), the total lumped dynamic cutting force vector $\boldsymbol{F}_{xyz}^{dc}(t)$ can be calculated in a similar fashion to Eqs. (1-2) by replacing $h_i^{st}(z,t)$ by $h_i^{dc}(z,t)$ and dropping the edge term $\boldsymbol{K}^e$, which comes from linearization of the total cutting force vector [6, 10]. These dynamic forces govern the stability of the cutter discussed next.

3.2. Dynamics and stability of serrated cutters

Assuming the tool to be rigid in the z direction, as it usually is, the generalized equation of motion for the serrated cutter can be described in the modal space as [6]:

$$\ddot{\boldsymbol{q}}(t) + \mathrm{diag}\left[2\zeta_r\omega_{n,r}\right]\dot{\boldsymbol{q}}(t) + \mathrm{diag}\left[\omega_{n,r}^2\right]\boldsymbol{q}(t) = \mathrm{diag}\left[\left(\frac{\omega_r^2}{k_r}\right)\right]\boldsymbol{F}_{xy}^{dc}(t), \quad (4)$$

wherein $\boldsymbol{q}(t)$is modal displacement vector, r are the number of modes, $\omega_{n,r}$, ζ_r, and k_r are the modal frequencies, damping ratios, and the stiffnesses, respectively, and $\boldsymbol{F}_{xy}^{dc}(t) = \begin{bmatrix} F_x^{dc} & F_y^{dc} \end{bmatrix}^T$ is the lumped force matrix. Eq. (4) represents the delay differential equations that are solved using the semi-discretization method [6, 10] to predict stability.

Having briefly described the static force model and the chatter stability model for serrated cutters, geometries of the standard and non-standard cutters of interest are discussed next.

4. Geometry of the standard and non-standard serrated end mills of interest

Force and stability models are governed by tool geometry. Since cutting tool manufacturers' that make serrated cutters do not describe their detailed geometry, we reconstruct geometric models for the two serrated tools of interest by scanning them in an Alicona make 3D optical surface profilometer. Details of the scanning process, and procedures to reconstruct geometry from scanned data using parametric definitions are presented in [9], and, for want of space, are not repeated herein, and the interested reader is directed to [4, 9] for details. The measured serration parameters and key geometric angles like the pitch angle ($\varphi_{p,i}$), the helix angle (η), and the initial phase shifts (ψ) between the waves on subsequent flutes for the standard trapezoidal profiled serrated cutter and the non-standard inclined-circular profiled serrated cutter are listed in Table 1.

Table 1. Geometry of the standard and non-standard serrated end mills.

Serration profile and classification; Tool make and model	Serration geometry; Initial phase shift (ψ); helix angles (η); pitch angles ($\varphi_{p,i}(0)$); No. of teeth (N);
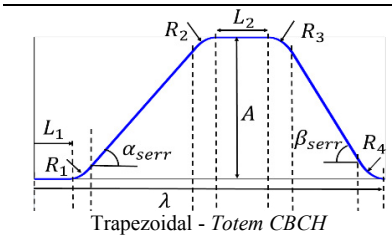 Trapezoidal - *Totem CBCH*	A = 0.63 mm; L_1 = 0.97 mm; L_2 = 0 mm; R_1 = 0.06 mm; R_2 = 0.39 mm; R_3 = 0.39 mm; R_4 = 0.06 mm; α_{serr} = 39°; β_{serr} = 40°; λ = 2.82 mm ψ = [0 120 240]° cw; η = [40 40 40]°; $\varphi_{p,i}(0)$ = [120 120 120]°; N = 3.
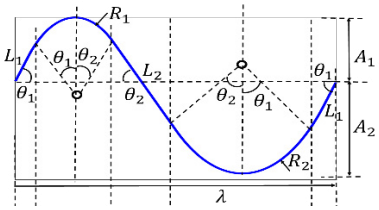 Inclined circular - *Iscar ERC160E32-3W16*	A = 0.48 mm; R_1 = 0.52 mm; R_2 = 0.90 mm; θ_1 = 40°; θ_2 = 32°; λ = 2.27 mm; L_1 = 0.11 mm; L_2 = 0.33 mm; ψ = [0 120 240]° cw; η = [38 38 38]°; $\varphi_{p,i}(0)$ = [120 120 120]°; N = 3.

5. Experimental validation of cutting forces and stability

This section first discusses the experimental validation of cutting forces, followed by validation of the stability models. The measured geometries listed in Table 1 were used in predictions. We cut Al7075 and use the following mechanistically identified cutting force coefficients: K_t^c=824 N/mm^2, K_r^c =225 N/mm^2, K_a^c =15 N/mm^2, K_t^e =24 N/mm, K_r^e =28 N/mm, K_a^e =2 N/mm. These were identified using a regular end mill.

The proposed static force model was previously validated experimentally in [4, 9] and those results for forces in F_x and F_y directions are reproduced in Fig. 2 for completeness. Results in Fig. 2 are for a 50% up-milling engagement condition with the feed at 0.05 mm/tooth/rev. Results with the trapezoidal profiled cutter are reported at 6000 RPM and with a depth of cut of 2 mm, whereas results for the inclined-circular profiled cutter are reported at 3000 RPM and with a depth of cut of 2.7 mm. Because cutting conditions for both cutters are different, a direct comparison between both is not possible, and that is separately discussed in Section 6. However, as is evident from Fig. 2, because model predicted and measured forces match well, the geometric models may be considered to be correct.

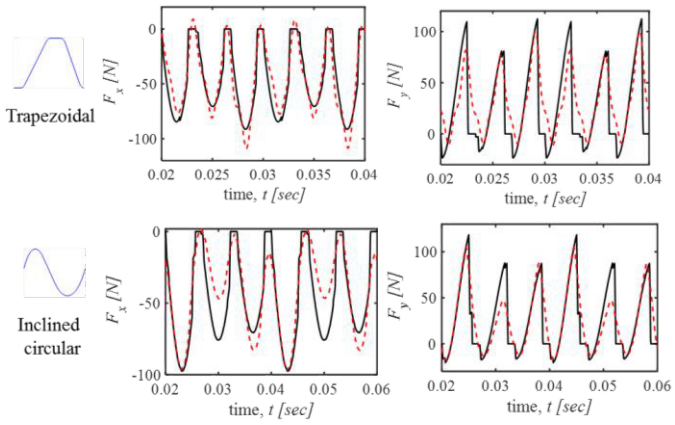

Fig. 2. Comparison of modelled (solid line) and measured (dashed line) cutting forces for the standard trapezoidal profiled serrated cutter (top) and the non-standard inclined-circular profiled serrated cutter (bottom).

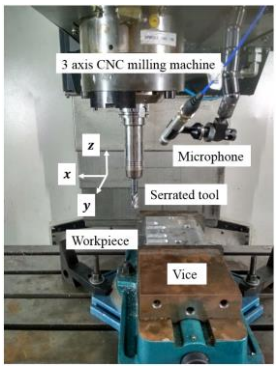

Fig. 3. Experimental setup to validate chatter stability predictions

Table 2. Measured dynamics

Modal parameters	Cutter type	
	Standard	Non-standard
f_x (Hz)	604.5	596
ζ_x (%)	1.7	1.76
k_x (N/m)	1.68E+7	1.93E+7
f_y (Hz)	603.7	617.5
ζ_y (%)	1.67	1.21
k_y (N/m)	1.49E+7	1.94E+7

The experimental setup to validate stability is shown in Fig. 3. The tools were mounted in a hydraulic tool holder and the stick-out from the holder's face was kept at 68 mm in both cases. Dynamics were measured and exhibited only one dominant mode in each direction for each cutter. Since the semi-discretization method stability predictions rely on dynamics characterized by modal parameters, those were extracted from the measured dynamics using CutPro®, and are listed in Table 2.

Stability was predicted using the model described in Section 3 using the measured dynamics and the coefficients listed earlier. Full engagement cutting, i.e., slotting was considered and the feed was taken to be 0.05 mm/tooth/rev. Experiments were conducted to test the boundaries of stability. The stable cutting case was identified as that for which the FFT of the audio signal is dominated by the tooth passing frequency and/or its harmonics. The chatter case was flagged as that in which the FFT of the audio signal is dominated by a frequency close to the natural frequency of the tool. Results for both tools are shown below – Fig. 4(a) shows results for the standard cutter and Fig. 4(b) shows results for the non-standard cutter.

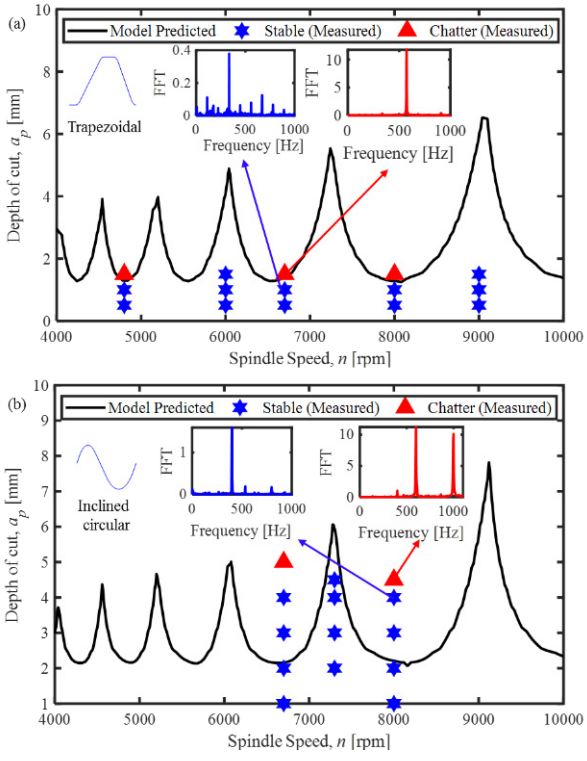

Fig. 4. Experimental validation of chatter stability for (a) standard trapezoidal serrated cutter and (b) non-standard inclined-circular serrated cutter.

As is evident from Fig. 4(a), experiments at different speeds confirms the correctness of the model predictions. Representative spectra for a stable and unstable cutting condition shown within Fig. 4(a) confirm that for cutting at a speed of 6700 rpm and at an axial depth of cut of 1 mm, the spectra shows the tooth passing frequency of 335 Hz, whereas for cutting at the same speed at a higher depth of cut of 1.5 mm, the spectra contains a peak corresponding to the natural frequency of the system – confirming the presence of chatter.

Similarly from Fig. 4(b) – which shows results for the non-standard cutter, representative spectra for the stable cut at 8000 RPM for a depth of cut of 4 mm only contains the tooth passing freqeucny of 400 Hz, and the spectra for cutting at the same speed, but at a higher depth of cut of 4.5 mm contains a dominant peak at ~599 Hz, which is near the mode of the tool. As is evident from Fig. 4(b), predicted stability boundaries are lower than the experimentally determined stability limits. Since the cutting force comparisons suggest that the geometric model for the non-standard profiled cutter is correct, these large discrepancies are thought to be due to potential uncertainties in correctly estimating the tool point dynamics – which needs to be addressed separately and appropriately.

6. Comparisons of cutting forces and stability of standard and non-standard profiled serrated end mills

This section discusses comparisons of simulated resultant cutting forces $\left(F_{xy} = \sqrt{F_x^2 + F_y^2}\right)$ and stability limits for the trapezoidal cutter with the inclined-circular cutter. For comparisons herein, cutting conditions and dynamics for both cutters are assumed to be the same. For all comparisons herein, all geometric parameters for both cutters are kept same as reported in Table 1. The cutting force coefficients are also taken to be same as earlier.

For force comparisons, 50% engagement up-milling cutting is considered at a speed of 6000 RPM with an axial depth of cut of 1 mm, and a feed of 0.05 mm/tooth/rev. For comparing stability, the same engagement conditions and feeds are considered. Since stability results presented in Section 5 were for cutters with different dynamics, to isolate the influence of serration geometry on stability, dynamics for both cutters are chosen arbitrarily to be the same as: $f_x = f_y$ =600 Hz, $\zeta_x = \zeta_y = 0.15$, $k_x = k_y = 6 \times 10^6$ N/m. Simulated cutting forces and stability boundaries for the same cutting conditions and for the dynamics of both cutters also being the same are compared in Fig. 5.

From Fig. 5(a) we observe that the peak resultant force for the non-standard inclined-circular profiled serrated cutter is 8% lower than the standard trapezoidal profiled cutter. And, from Fig. 5(b), we see that the stability boundaries for both cutters are similar.

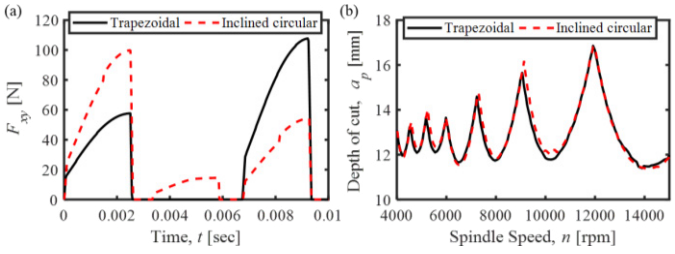

Fig. 5. Comparisons of (a) resultant forces and (b) stability limits for standard trapezoidal and non-standard inclined-circular profiled serrated cutters.

These results for the stability with different serration geometries being the same are in line with what was also reported in [3], wherein it was also shown that for serrated cutters with optimized sinusoidal, circular, and trapezoidal profiles, and for cutters with uniform dynamics, the stability behavior is also the same.

7. Conclusions and outlook

The main objective of this work was to compare the cutting force and chatter-free stability behavior of a standard trapezoidal serrated cutter with that of a non-standard inclined-circular serrated cutter. Geometric models for both cutters were first validated by comparing predicted forces and stability with measurements. While forces compare well, slight discrepancies in stability behavior for the non-standard cutter were observed, and that needs to be addressed appropriately.

To isolate the influence of serration geometry on forces and stability, subsequent simulation-based comparisons that assume the same dynamics and cutting conditions for both cutters, we found that from the perspective of selection of cutters that preferentially reduce forces, the non-standard profiled cutter might make for a better choice, whereas, from the consideration of selecting cutters to maximize chatter-free stability limits, since both cutters exhibit similar stability behavior, any of the two cutters may be selected.

Results herein suggest that even though the non-standard profiled serrated cutter marginally outperforms the standard profiled serrated cutter, there is clearly an opportunity to optimize serration geometries such as to help reduce process forces and maximize the potential for chatter-free cutting. This indeed forms part of our ongoing and planned future work.

Acknowledgements

The first author gratefully acknowledges the Shastri Indo-Canadian Institute for supporting his summer 2019 research stay at the University of British Columbia under the supervision of Dr. Murat Kilic and Prof. Yusuf Altintas. The authors also acknowledge partial support for experiments by the Government of India's Impacting Research Innovation and Technology initiative through project number IMPRINT 5509.

References

[1] Stone B. Chatter and Machine Tools. *Springer*, 2014.
[2] Tlusty J, et al. Use of Special Milling Cutters against Chatter. *Proceedings of the NAMRC.* 1983; 11: 408–415.
[3] Tehranizadeh F, et al. Investigating effects of serration geometry on milling forces and chatter stability for their optimal selection. *Int. J. Mach. Tool. Manu.* 2019; 144.
[4] Bari P, et al. Improved chip thickness model for serrated end milling. *CIRP J. Manuf. Sci. Tec.* 2019; 25: 36-49.
[5] Merdol S D, Altintas Y. Mechanics and dynamics of serrated cylindrical and tapered end mills. *J. Manuf. Sci. Eng.* 2004; 126 (2): 317.
[6] Dombovari Z, et al. The effect of serration on mechanics and stability of milling cutters. *Int. J. Mach. Tool. Manu.* 2010; 50 (6): 511–520.
[7] No T, et al. Force and stability modeling for non-standard edge geometry end mills. *J. Manuf. Sci. Eng.* 2019;141: 121002-1.
[8] Burek J, et al. The influence of the cutting edge shape on high performance cutting. *Aircr. Eng. Aerosp. Tec.* 2018; 90/1: 134–145.
[9] Bari P, et al. Geometric models of non-standard serrated end mills. *Int. J. Adv. Manuf. Tech.* 2020. (*in press*)
[10] Insperger T, Stépán G. Semi-Discretization for Time-Delay Systems. *Appl. Math.* 2011.